Locating Complex Double-Line-to-Ground Faults: Theory and Field Case Study

Steven Chase and Sumit Sawai, *Schweitzer Engineering Laboratories, Inc.*
Douglas Taylor, *Avista Utilities*

***Abstract*—A double-line-to-ground (DLG) fault is typically modeled as a short-circuit connection from two phases (i.e., Phases A and B) to a common point, with a fault resistance from the common point to ground. Traditional impedance-based fault location algorithms work properly when the fault matches this standard topology, and they are potentially challenged when it does not.**

This paper presents a generalized representation of a DLG fault with three distinct fault resistances: two from the faulted phases to the common point and one from the common point to the ground. The paper shows how to locate these DLG faults by solving voltage loop equations written in the phase domain, using A, B, and C components rather than symmetrical components. The solution of the loop equations yields the per-unit fault location and the three resistance values. This approach is somewhat unique since the fault resistance calculation is inherently a part of the fault location process. The paper analyzes several other DLG fault topologies as well.

The proposed fault location method uses data from event reports stored by relays at both ends of a transmission line. Thus, it is a non-real-time solution that can be used for particularly challenging cases in which the results of traditional methods are in doubt. The method can be used regardless of whether the relays are supplied with a GPS time signal, although the solution is simpler when a common time reference is available. Time synchronization is not required for a radial line.

To validate the fault locator, the paper analyzes a field case involving a radial 115 kV line on the Avista Utilities transmission network. In this event, the fault begins as a single-line-to-ground fault on A-phase (AG fault) and then evolves into a DLG fault involving A- and B-phases (ABG fault with nonstandard topology).

I. Double-Line-to-Ground (DLG) Fault Location and Limitations of Standard Methods

Most of the faults that occur in the power system are unsymmetrical faults; namely, single-line-to-ground (SLG), line-to-line (LL), and DLG faults, with DLG faults being the rarest out of the three [1]. In the typical textbook analysis of DLG faults, the resistances between the faulted phases and the common point are assumed to be negligible, and only the resistance from the common point to ground is considered [1] [2]. This assumption may not hold true in practice, as not all the DLG faults have negligible fault resistance between the faulted phases. However, this assumption greatly simplifies the fault analysis in the symmetrical component technique. Standard single-ended, impedance-based fault location techniques, such as the Takagi method, provide accurate results for SLG and LL faults on a homogeneous and transposed system. For DLG faults, if the resistances from the faulted phases to the common point are negligible, the standard techniques can produce accurate results. However, if the resistances are not negligible, the accuracy of the standard techniques can be compromised.

To understand why DLG faults challenge fault location algorithms, we are going to look at an example of an ABG fault on a simple unloaded radial system with a perfectly transposed line as shown in Fig. 1.

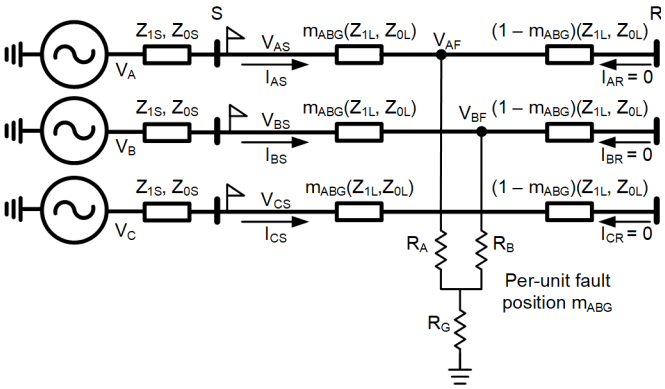

Fig. 1. Signals recorded by relays for an ABG fault on a radial transmission line.

A fault locating device (protective relay) is marked by a flag near Bus S. V_{AS}, V_{BS} and V_{CS} are the voltage phasors measured by the relay, and I_{AS}, I_{BS} and I_{CS} are the current phasors measured by the relay. The system voltage sources V_A, V_B, and V_C drive the circuit on the S-side. The S-side system source has positive-sequence impedance Z_{1S} and zero-sequence impedance Z_{0S}, and the transmission line has positive-sequence and zero-sequence impedances of Z_{1L} and Z_{0L}, respectively. The per-unit distance to the fault is m_{ABG}, R_A, R_B and R_G are the fault resistances.

Kirchhoff's voltage law (KVL) equations for the AB loop (starting from the relay location) are (1) and (2):

$$V_{AS} - V_{BS} = m_{ABG}\, Z_{1L} \left(I_{AS} - I_{BS}\right) + V_{AF} - V_{BF} \tag{1}$$

$$V_{AF} - V_{BF} = R_A\, I_{AS} - R_B\, I_{BS} \tag{2}$$

We multiply (1) by the complex conjugate of a phasor quantity referred to as a polarizing quantity (pol). The asterisk symbol (*) denotes complex conjugation. If the polarizing quantity is chosen properly, the multiplication with pol* moves the term $V_{AF} - V_{BF}$ (fault point voltage) to the real axis; in other words, the imaginary part of the resulting quantity is zero, as shown in (3).

$$\mathrm{Im}\left[\left(R_A\, I_{AS} - R_B\, I_{BS}\right) \mathrm{pol}^*\right] = 0 \tag{3}$$

From (1) and (3), we can derive (4), which is the general fault location equation for AB, ABG, and ABC faults.

$$m_{ABG} = \frac{\mathrm{Im}\left(V_{ABS}\, pol^{*}\right)}{\mathrm{Im}\left(Z_{1L} I_{ABS}\, pol^{*}\right)} \tag{4}$$

Now the question remains as to which phasor should be selected for the polarizing quantity. Table I shows three possible candidates, the best of which is the phasor quantity that closely meets the criterion of (3).

TABLE I
POLARIZING QUANTITIES FOR ABG FAULT

Option	Polarizing Quantity	Description
1	I_{ABS2}	Negative-sequence current referred to faulted phases
2	I_{ABS}	Phase-to-phase current of faulted phases
3	I_{0S}	Zero-sequence current

Looking at (3), we see that there are three separate cases for the fault resistances, about which we can make the following observations:

Case 1) $R_A = R_B = 0$. For this case, any polarizing quantity can produce correct results, since $V_{AF} - V_{BF} = 0$ and (1) can be directly solved for the single unknown, which is the fault location.

Case 2) $R_A = R_B = R_F$. Here, (3) simplifies into (5).

$$\mathrm{Im}\left[\left(R_F I_{ABS}\right)\left(pol\right)^{*}\right] = 0 \tag{5}$$

In (5), the fault point voltage ($V_{AF} - V_{BF} = R_F I_{ABS}$) is at the same angle as Current I_{ABS}. Thus, the term $(R_F I_{ABS})(I_{ABS})^*$ has an imaginary part equal to zero. This makes Current I_{ABS} the correct choice of polarizing quantity for both AB and ABG faults. For an AB fault, I_{ABS2} can also function as a correct polarizing quantity. $I_{AS} + I_{BS} = 0$ for an AB fault, which means that I_{ABS} is in phase with I_{ABS2}, as seen in Fig. 2. But for an ABG fault, $I_{AS} + I_{BS} \neq 0$, meaning that Phasor I_{ABS2} is not generally in phase with I_{ABS}.

The phase angle relationship between the fault point voltage and I_{ABS2} depends on the fault resistance and the fault location for an ABG fault. Therefore, I_{ABS2} is not always a suitable polarizing quantity for ABG faults.

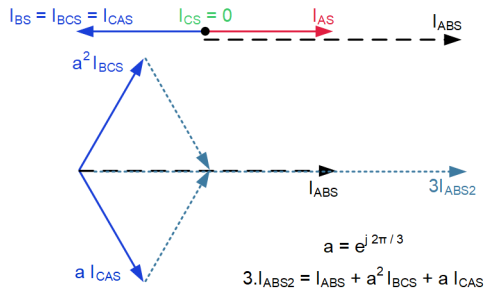

Fig. 2. Negative-sequence current I_{ABS2} during AB fault on system of Fig. 1.

The third polarizing option of zero-sequence current (I_0) does not work for an AB fault since the fault does not produce any I_0. For an ABG fault, the angle of the resulting I_0 depends on the fault location and involved fault resistances, resulting in a lack of a fixed phase angle relationship between the fault point voltage and I_0. Therefore, I_0 is not a suitable polarizing quantity for ABG faults.

Case 3) $R_A \neq R_B \neq 0$. In this case, for an AB fault, the observations made in Case 2 still hold true, and either I_{ABS} or I_{ABS2} can function as a correct polarizing quantity. But none of the quantities listed in Table I work correctly for an ABG fault, since both R_{AF} and R_{BF} are unknowns, and the resulting term $(R_A I_{AS} - R_B I_{BS})$ does not have a definite phase angle relation with any of the candidate polarizing quantities. To determine the fault location for this type of fault requires solving a system of equations for all of the unknowns (fault location and fault resistances). The system of KVL equations can be written either in the phase domain network or in the symmetrical component domain (sequence domain) network.

We attempt to solve equations in the sequence domain first. Fig. 3 is a representation of the system of Fig. 1 in the symmetrical component domain [3].

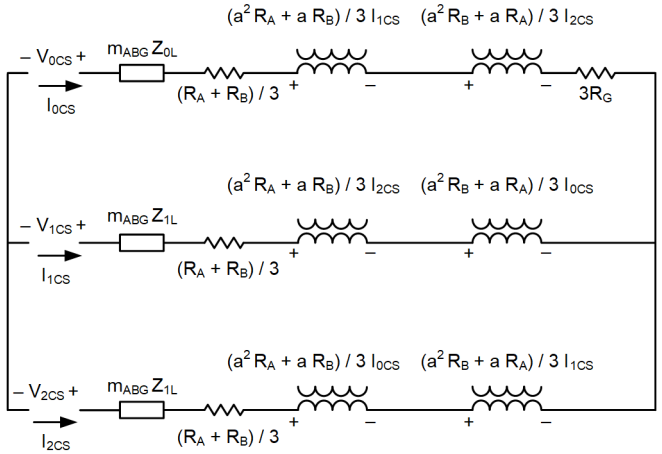

Fig. 3. ABG fault representation in the sequence network.

In Fig. 3, voltage and current phasors (V_{0CS}, V_{1CS}, V_{2CS}, I_{0CS}, I_{1CS}, I_{2CS}) are available from the relay measurements, and the fault location and the fault resistances are the unknown variables.

It is important to note here that the unknown quantities are real numbers and not complex numbers. This allows us to solve for all four unknowns (m_{ABG}, R_A, R_B and, R_G) by writing two complex-valued KVL equations that can be split into real and imaginary parts to form four real-valued equations in total. Equation (6) is the matrix representation of the resulting KVL equations.

$$\begin{bmatrix} m_{ABG} \\ R_A \\ R_B \\ R_G \end{bmatrix} = [M]^{-1}[V] \tag{6}$$

where:

M is a 4 by 4 matrix of system impedances and Bus S currents.

V is a 4 by 1 matrix of Bus S voltages.

From Fig. 3, it is evident that the sequence networks are mutually coupled, and this substantially nullifies the benefit of using symmetrical components (i.e., decoupling of the sequence networks). Also in practice, transmission lines may not be perfectly transposed, or they may be untransposed. This results in further coupling between the sequence networks. Since general ABG fault analysis inevitably involves solving a coupled system, it is arguably more convenient to solve in the phase domain in terms of (A, B, C) components. Sections III and IV discuss phase domain analysis of general ABG faults, but first, we discuss the process of checking fault location results in Section II.

II. Using Event Report Data to Check the Results of DLG-Fault-Locating Algorithms

When a DLG fault occurs on a transmission line within the protection zone, a modern protective relay issues a trip, calculates a fault location, and records an event report. If the fault location result is in doubt, it can be checked using event report data from both ends of the transmission line (see Fig. 4). In Fig. 4, the transmission line is transposed and has self-impedance, Z_S, and mutual impedance, Z_M. With minor modifications, the methods described in this paper can be applied to untransposed lines as well. The relay locations are shown as flags at the S and R Terminals.

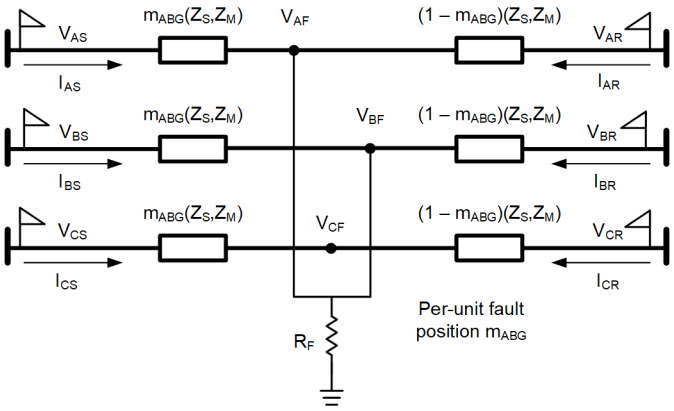

Fig. 4. Signals recorded by relays for a DLG fault on a transmission line.

S-terminal signals (V_{AS}, V_{BS}, V_{CS}, I_{AS}, I_{BS}, I_{CS}) and R-terminal signals (V_{AR}, V_{BR}, V_{CR}, I_{AR}, I_{BR}, I_{CR}) are taken from relay event reports after the fault has occurred. If the data from the two ends are synchronized to a common time source (such as GPS), we can easily establish a common angular reference for both sets of data. Later sections describe how to use unsynchronized data for fault location purposes.

To check the quality of the relay fault location result, we compare the values of fault voltages V_{AF}, V_{BF}, and V_{CF} calculated from the S-terminal and R-terminal and verify that they match. In the following equations, m_{ABG} is the per-unit fault location given by the S-terminal relay.

$$V_{AF\_S} = V_{AS} - m_{ABG}\left[Z_S I_{AS} + Z_M\left(I_{BS} + I_{CS}\right)\right] \quad (7)$$

$$V_{BF\_S} = V_{BS} - m_{ABG}\left[Z_S I_{BS} + Z_M\left(I_{AS} + I_{CS}\right)\right] \quad (8)$$

$$V_{CF\_S} = V_{CS} - m_{ABG}\left[Z_S I_{CS} + Z_M\left(I_{AS} + I_{BS}\right)\right] \quad (9)$$

$$V_{AF\_R} = V_{AR} - \left(1 - m_{ABG}\right)\left[Z_S I_{AR} + Z_M\left(I_{BR} + I_{CR}\right)\right] \quad (10)$$

$$V_{BF\_R} = V_{BR} - \left(1 - m_{ABG}\right)\left[Z_S I_{BR} + Z_M\left(I_{AR} + I_{CR}\right)\right] \quad (11)$$

$$V_{CF\_R} = V_{CR} - \left(1 - m_{ABG}\right)\left[Z_S I_{CR} + Z_M\left(I_{AR} + I_{BR}\right)\right] \quad (12)$$

If (13) holds true, the quality checks pass (where |•| denotes the absolute value of a complex number):

$$\left|V_{AF\_S} - V_{AF\_R}\right| + \left|V_{BF\_S} - V_{BF\_R}\right| + \left|V_{CF\_S} - V_{CF\_R}\right| \approx 0 \quad (13)$$

If these quality checks do not pass, the actual fault topology may differ from the standard fault topology. In such a case, one may solve for the fault location assuming a nonstandard topology and see if that analysis yields better results. In the following sections, we examine several nonstandard DLG fault topologies.

III. Generalized DLG Fault Analysis (Topology 1)

The first nonstandard DLG fault topology we analyze, Topology 1 (T1), is a generalization of the classic DLG fault, containing three fault resistances as shown in Fig. 5. For an ABG fault, there are four real-valued unknowns to solve for: fault resistances R_A, R_B, and R_G, and per-unit fault position m_{ABG}. With data from both ends of the line, it is possible to solve for m_{ABG} without calculating the values of the fault resistances. However, if the fault is on a radial line and only one event report is available, the fault resistance must be incorporated into the solution to complete the KVL loops. We present a general solution for a two-source system that incorporates the fault resistance and only requires trivial modifications for application to radial lines. Including fault resistance calculations as part of fault location can yield additional information and insight regarding the nature of power system faults.

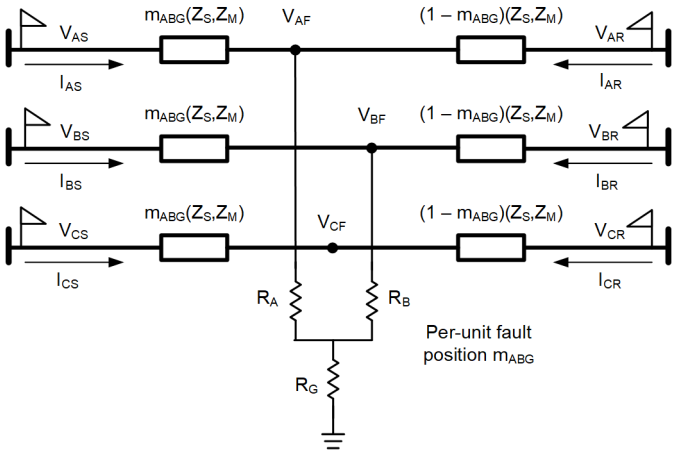

Fig. 5. Generalized DLG circuit representation of an ABG fault.

$$V_{AS} - m_{ABG}\left[Z_s I_{AS} + Z_M\left(I_{BS} + I_{CS}\right)\right] - R_A\left(I_{AS} + I_{AR}\right) - R_G\left(I_{AS} + I_{AR} + I_{BS} + I_{BR}\right) = 0 \quad (14)$$

$$V_{BS} - m_{ABG}\left[Z_s I_{BS} + Z_M\left(I_{AS} + I_{CS}\right)\right] - R_B\left(I_{BS} + I_{BR}\right) - R_G\left(I_{AS} + I_{AR} + I_{BS} + I_{BR}\right) = 0 \quad (15)$$

$$\mathrm{Re}(V_{AS}) = m_{ABG}\,\mathrm{Re}\left[Z_S I_{AS} + Z_M\left(I_{BS} + I_{CS}\right)\right] + R_A\,\mathrm{Re}\left(I_{AS} + I_{AR}\right) + R_G\,\mathrm{Re}\left(I_{AS} + I_{AR} + I_{BS} + I_{BR}\right) \quad (16)$$

$$\mathrm{Im}(V_{AS}) = m_{ABG}\,\mathrm{Im}\left[Z_S I_{AS} + Z_M\left(I_{BS} + I_{CS}\right)\right] + R_A\,\mathrm{Im}\left(I_{AS} + I_{AR}\right) + R_G\,\mathrm{Im}\left(I_{AS} + I_{AR} + I_{BS} + I_{BR}\right) \quad (17)$$

$$\mathrm{Re}(V_{BS}) = m_{ABG}\,\mathrm{Re}\left[Z_S I_{BS} + Z_M\left(I_{AS} + I_{CS}\right)\right] + R_B\,\mathrm{Re}\left(I_{BS} + I_{BR}\right) + R_G\,\mathrm{Re}\left(I_{AS} + I_{AR} + I_{BS} + I_{BR}\right) \quad (18)$$

$$\mathrm{Im}(V_{BS}) = m_{ABG}\,\mathrm{Im}\left[Z_S I_{BS} + Z_M\left(I_{AS} + I_{CS}\right)\right] + R_B\,\mathrm{Im}\left(I_{BS} + I_{BR}\right) + R_G\,\mathrm{Im}\left(I_{AS} + I_{AR} + I_{BS} + I_{BR}\right) \quad (19)$$

We start by writing the two complex-valued voltage drop equations, (14) and (15), for the faulted phases (A and B), starting at the S-terminal relay and going through the fault.

We split the two complex-valued equations into real and imaginary parts to yield a system of the four real-valued linear equations, (16), (17), (18), and (19), to solve for m_{ABG}, R_A, R_B, and R_G. Re() and Im() denote the real and imaginary parts of complex numbers.

While solving for the four unknowns, the voltage drops between the fault and the R-terminal are not accounted for. Having solved for m_{ABG}, R_A, R_B, and R_G, the quality checks from Section II can now be applied to provide additional confidence in the solution.

IV. Simultaneous SLG Faults (Topology 2)

The second topology we analyze, Topology 2 (T2), consists of two simultaneous SLG faults within the protection zone, as shown in Fig. 6. For simultaneous AG and BG faults, there are four real-valued unknowns to solve for: the fault resistances R_{AG} and R_{BG} and the per-unit fault positions m_{AG} and m_{BG}. In this case, the AG fault is closer to the S-terminal than the BG fault. For the case in which the BG fault is closer than the AG fault, the analysis is similar, although some modifications are required.

As previously mentioned, if the data from the two ends are synchronized to a common time source (such as GPS), we can easily establish a common angular reference for both sets of data, permitting a linear algebra solution.

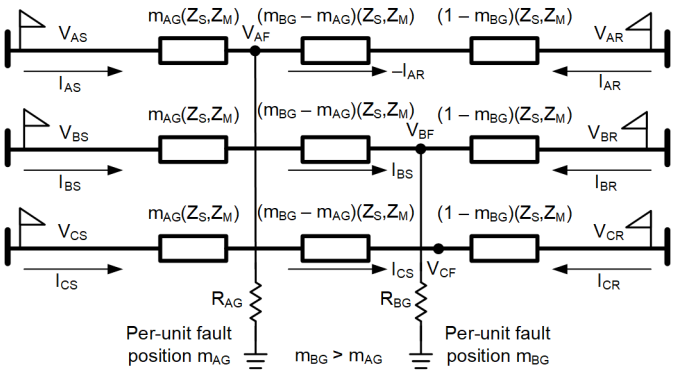

Fig. 6. Simultaneous AG and BG faults.

We start by writing two complex-valued voltage drop equations for the faulted phases (A and B), starting at the S-terminal relay, (20) and (21).

We rearrange to get (22) and (23).

We split (22) and (23) into real and imaginary parts to yield a system of four real-valued linear equations to solve for m_{AG}, m_{BG}, R_{AG}, and R_{BG}, (24), (25), (26) and (27). Re() and Im() denote the real and imaginary parts of complex numbers. Unknowns m_{AG} and R_{AG} can be solved for separately using a 2 by 2 linear system, as desired.

$$V_{AS} - m_{AG}\left[Z_S I_{AS} + Z_M\left(I_{BS} + I_{CS}\right)\right] - R_{AG}\left(I_{AS} + I_{AR}\right) = 0 \quad (20)$$

$$V_{BS} - m_{AG}\left[Z_S I_{BS} + Z_M\left(I_{AS} + I_{CS}\right)\right] - \left(m_{BG} - m_{AG}\right)\left[Z_S I_{BS} + Z_M\left(-I_{AR} + I_{CS}\right)\right] - R_{BG}\left(I_{BS} + I_{BR}\right) = 0 \quad (21)$$

$$V_{AS} = m_{AG}\left[Z_S I_{AS} + Z_M\left(I_{BS} + I_{CS}\right)\right] + R_{AG}\left(I_{AS} + I_{AR}\right) \quad (22)$$

$$V_{BS} = m_{AG}\,Z_M\left(I_{AS} + I_{AR}\right) + m_{BG}\left[Z_S I_{BS} + Z_M\left(-I_{AR} + I_{CS}\right)\right] + R_{BG}\left(I_{BS} + I_{BR}\right) \quad (23)$$

$$\mathrm{Re}(V_{AS}) = m_{AG}\,\mathrm{Re}\left[Z_S I_{AS} + Z_M\left(I_{BS} + I_{CS}\right)\right] + R_{AG}\,\mathrm{Re}\left(I_{AS} + I_{AR}\right) \quad (24)$$

$$\mathrm{Im}(V_{AS}) = m_{AG}\,\mathrm{Im}\left[Z_S I_{AS} + Z_M\left(I_{BS} + I_{CS}\right)\right] + R_{AG}\,\mathrm{Im}\left(I_{AS} + I_{AR}\right) \quad (25)$$

$$\mathrm{Re}(V_{BS}) = m_{AG}\,\mathrm{Re}\left[Z_M\left(I_{AS} + I_{AR}\right)\right] + m_{BG}\,\mathrm{Re}\left[Z_S I_{BS} + Z_M\left(-I_{AR} + I_{CS}\right)\right] + R_{BG}\,\mathrm{Re}\left(I_{BS} + I_{BR}\right) \quad (26)$$

$$\mathrm{Im}(V_{BS}) = m_{AG}\,\mathrm{Im}\left[Z_M\left(I_{AS} + I_{AR}\right)\right] + m_{BG}\,\mathrm{Im}\left[Z_S I_{BS} + Z_M\left(-I_{AR} + I_{CS}\right)\right] + R_{BG}\,\mathrm{Im}\left(I_{BS} + I_{BR}\right) \quad (27)$$

$$V_{AF\_S} = V_{AS} - m_{AG}\left[Z_S I_{AS} + Z_M\left(I_{BS} + I_{CS}\right)\right] \tag{28}$$

$$V_{BF\_S} = V_{BS} - m_{AG}\left[Z_S I_{BS} + Z_M\left(I_{AS} + I_{CS}\right)\right] - \left(m_{BG} - m_{AG}\right)\left[Z_S I_{BS} + Z_M\left(-I_{AR} + I_{CS}\right)\right] \tag{29}$$

$$V_{CF\_S} = V_{CS} - m_{AG}\left[Z_S I_{CS} + Z_M\left(I_{AS} + I_{BS}\right)\right] - \left(m_{BG} - m_{AG}\right)\left[Z_S I_{CS} + Z_M\left(-I_{AR} + I_{BS}\right)\right] \tag{30}$$

$$V_{AF\_R} = V_{AR} - \left(1 - m_{BG}\right)\left[Z_S I_{AR} + Z_M\left(I_{BR} + I_{CR}\right)\right] - \left(m_{BG} - m_{AG}\right)\left[Z_S I_{AR} + Z_M\left(-I_{BS} + I_{CR}\right)\right] \tag{31}$$

$$V_{BF\_R} = V_{BR} - \left(1 - m_{BG}\right)\left[Z_S I_{BR} + Z_M\left(I_{AR} + I_{CR}\right)\right] \tag{32}$$

$$V_{CF\_R} = V_{CR} - \left(1 - m_{BG}\right)\left[Z_S I_{CR} + Z_M\left(I_{AR} + I_{BR}\right)\right] \tag{33}$$

While solving for the four unknowns, not all line voltage drops are accounted for. As a final quality check, we compare the values of fault voltages V_{AF}, V_{BF}, and V_{CF} calculated from the S-terminal and R-terminal to verify that they match, using (28), (29), (30), (31), (32), and (33). Even though C-phase is not faulted, V_{CF} is defined as being the C-phase line voltage at position m_{BG} (see Fig. 6). At this point, the values of m_{AG}, m_{BG}, R_{AG}, and R_{BG} have been solved for and are known.

If (34) holds true, the quality checks pass:

$$\left|V_{AF\_S} - V_{AF\_R}\right| + \left|V_{BF\_S} - V_{BF\_R}\right| + \left|V_{CF\_S} - V_{CF\_R}\right| \approx 0 \tag{34}$$

V. Solving with Unsynchronized Data and Nonlinear System Equations

If the event reports from the line ends are not synchronized, the angle between V_{AS} and V_{AR} is an unknown that must be solved for, in addition to the fault position and fault resistance values. In the unsynchronized case, we can take the signal V_{AS} as the angle reference for all signals (from Terminals S and R). Define signals (V_{AR}', V_{BR}', V_{CR}', I_{AR}', I_{BR}', I_{CR}') as the R-terminal signals referenced to V_{AR} (with V_{AR}' having a phase angle of zero). Because the data from the two ends are not synchronized, the actual R-terminal signals (referenced to V_{AS}) can be expressed as in (35):

$$\begin{aligned} V_{AR} &= V_{AR}'\, e^{j\theta} \\ V_{BR} &= V_{BR}'\, e^{j\theta} \\ V_{CR} &= V_{CR}'\, e^{j\theta} \\ I_{AR} &= I_{AR}'\, e^{j\theta} \\ I_{BR} &= I_{BR}'\, e^{j\theta} \\ I_{CR} &= I_{CR}'\, e^{j\theta} \end{aligned} \tag{35}$$

These expressions for the R-terminal signals can be inserted into the fault location equations derived in Sections III and IV. The incorporation of the extra complex exponential term makes the equations nonlinear. Thus, iterative solution methods are required to locate complex DLG faults using unsynchronized data. Reference [4] presents an iterative solution that uses unsynchronized event report data to locate shunt faults with standard topologies.

If two AG faults occur simultaneously in the protection zone, there are effectively six real-valued unknowns (see Fig. 7). These are the two fault locations (m_{AG1} and m_{AG2}), the two fault resistances (R_{AG1} and R_{AG2}), and the real and imaginary components of the current I_{AX} between the faults (I_{AXR} and I_{AXI}).

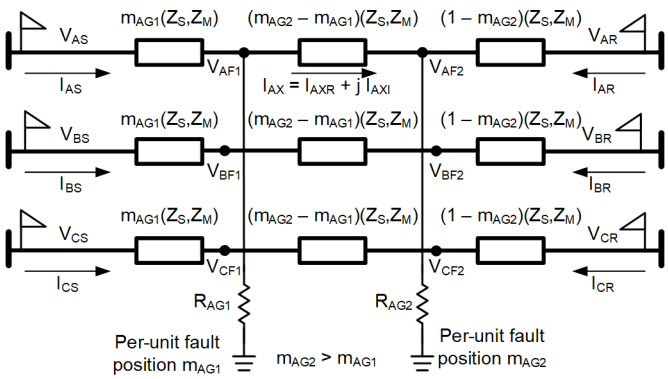

Fig. 7. Simultaneous AG faults within the protection zone.

Define the voltages at the fault points as follows:

$$V_{AF1} = V_{AS} - m_{AG1}\left[Z_S I_{AS} + Z_M\left(I_{BS} + I_{CS}\right)\right] \tag{36}$$

$$V_{BF1} = V_{BS} - m_{AG1}\left[Z_S I_{BS} + Z_M\left(I_{AS} + I_{CS}\right)\right] \tag{37}$$

$$V_{CF1} = V_{CS} - m_{AG1}\left[Z_S I_{CS} + Z_M\left(I_{AS} + I_{BS}\right)\right] \tag{38}$$

$$V_{AF2} = V_{AR} - \left(1 - m_{AG2}\right)\left[Z_S I_{AR} + Z_M\left(I_{BR} + I_{CR}\right)\right] \tag{39}$$

$$V_{BF2} = V_{BR} - \left(1 - m_{AG2}\right)\left[Z_S I_{BR} + Z_M\left(I_{AR} + I_{CR}\right)\right] \tag{40}$$

$$V_{CF2} = V_{CR} - \left(1 - m_{AG2}\right)\left[Z_S I_{CR} + Z_M\left(I_{AR} + I_{BR}\right)\right] \tag{41}$$

The values of m_{AG1}, m_{AG2}, R_{AG1}, R_{AG2}, I_{AXR}, I_{AXI} must satisfy the following equations.

$$V_{AF1} = R_{AG1}\left(I_{AS} - I_{AX}\right) \tag{42}$$

$$V_{AF2} = R_{AG2}\left(I_{AR} + I_{AX}\right) \tag{43}$$

$$V_{AF1} - \left(m_{AG2} - m_{AG1}\right)\left[Z_S I_{AX} + Z_M\left(I_{BS} + I_{CS}\right)\right] = V_{AF2} \tag{44}$$

$$V_{BF1} - \left(m_{AG2} - m_{AG1}\right)\left[Z_S I_{BS} + Z_M\left(I_{AX} + I_{CS}\right)\right] = V_{BF2} \tag{45}$$

$$V_{CF1} - \left(m_{AG2} - m_{AG1}\right)\left[Z_S I_{CS} + Z_M\left(I_{AX} + I_{BS}\right)\right] = V_{CF2} \tag{46}$$

We observe that these equations contain terms in which the unknown fault resistances R_{AG1} and R_{AG2} are multiplied by the unknown current I_{AX}. There are also terms in which the unknown fault locations m_{AG1} and m_{AG2} are multiplied by the unknown current I_{AX}. Thus, the equations are nonlinear and

must be solved iteratively, even if the relays at the two ends are synchronized by a common time source.

For the case of two simultaneous AG faults, the appropriate choice of an iterative solution method depends on whether the event report data are synchronized. With synchronized data, we can start with the complex-valued equations, (42), (43), and (44), and split these into real and imaginary parts, forming six real-valued equations to solve for the six unknown quantities (m_{AG1}, m_{AG2}, R_{AG1}, R_{AG2}, I_{AXR}, I_{AXI}). Since the number of equations matches the number of unknowns, a multivariate Newton-Raphson solution can be implemented in this case. Equations (45) and (46) can then be evaluated as quality checks.

With unsynchronized data, there is an additional synchronizing angle ($\boldsymbol{\theta}$) to solve for (see (35)). Thus, the seven unknowns in this case are m_{AG1}, m_{AG2}, R_{AG1}, R_{AG2}, I_{AXR}, I_{AXI}, and $\boldsymbol{\theta}$. We can only form even numbers of real-valued equations by writing complex-valued equations and splitting them into real and imaginary parts. Consequently, we cannot write seven real-valued equations to solve for the seven unknowns, and the system cannot be described by a square matrix. In this case, the standard multivariate Newton-Raphson technique cannot be used. Genetic algorithms and Gauss-Newton iteration are examples of solution methods that can be applied to systems of nonlinear equations in which the number of equations does not match the number of unknowns. See [5], [6], and [7] for more information on iterative numerical techniques. Section VI presents numerical results for both the synchronized and unsynchronized double-AG fault cases.

VI. Numerical Simulation Cases

The following three example cases illustrate the performance of the proposed solutions for ABG faults of T1 (general ABG) and T2 (simultaneous AG and BG), as well as for a fault consisting of two simultaneous AG faults within the protection zone. Faults were simulated for a transposed 100 kilometer and 230 kV transmission line in the real-time digital simulator (RTDS). Line parameters Z_{1L} = 32.48 at 87.10 degrees and Z_{0L} = 139.66 at 75.31 degrees (primary ohms) were used.

In the first two cases, three solutions were run, each with an associated quality check or error term (in primary volts), derived using equations similar to (13) from Section II. In both of these cases, only one solution calculates the fault correctly (the solution corresponding to the actual fault topology), and it has an error term much smaller than those of the other two methods. The error term for the successful solution is also very small compared to the system voltage. Comparison of the error quantities permits a rough determination of the fault topology in each case. Results are given to two significant figures.

A. Generalized ABG Fault With Synchronized Data

An ABG fault of T1 (general ABG) is simulated at 0.3 pu of line length with R_A = 10 ohms primary, R_B = 1 ohm primary, and R_G = 2 ohms primary. Results for the different algorithms are shown in Table II, Table III, and Table IV.

TABLE II
GENERAL ABG FAULT—I_{AB} POLARIZATION RESULTS

Calculated Fault Parameters	Results with Traditional Double-Ended I_{AB} Polarization
m_{ABG} (pu)	0.21
Error (kV primary)	16

TABLE III
GENERAL ABG FAULT—T1 SOLUTION RESULTS

Calculated Fault Parameters	Results of T1 Solution
m_{ABG} (pu)	0.29
R_A (ohms primary)	10
R_B (ohms primary)	1.2
R_G (ohms primary)	2.3
Error (kV primary)	1.6

TABLE IV
GENERAL ABG FAULT—T2 SOLUTION RESULTS

Calculated Fault Parameters	Results of T2 Solution
m_{AG} (pu)	0.22
m_{BG} (pu)	0.22
R_{AG} (ohms primary)	12
R_{BG} (ohms primary)	3.9
Error check (kV primary)	14

B. Simultaneous AG and BG Faults With Synchronized Data

Simultaneous AG and BG faults (T2) are simulated at 0.3 pu and 0.7 pu of the line length, respectively. Fault resistances are R_{AG} = 20 ohms primary and R_{BG} = 10 ohms primary. Results for the different solutions are shown in Table V, Table VI, and Table VII.

TABLE V
SIMULTANEOUS AG AND BG FAULTS—I_{AB} POLARIZATION RESULTS

Calculated Fault Parameters	Results with Traditional Double-Ended I_{AB} Polarization
m_{ABG} (pu)	0.56
Error (kV primary)	55

TABLE VI
SIMULTANEOUS AG AND BG FAULTS—T1 SOLUTION RESULTS

Calculated Fault Parameters	Results of T1 Solution
m_{ABG} (pu)	0.51
R_A (ohms primary)	15
R_B (ohms primary)	20
R_G (ohms primary)	6.7
Error check (kV primary)	54

TABLE VII
SIMULTANEOUS AG AND BG FAULTS—T2 SOLUTION RESULTS

Calculated Fault Parameters	Results of T2 Solution
m_{AG} (pu)	0.28
m_{BG} (pu)	0.70
R_{AG} (ohms primary)	20
R_{BG} (ohms primary)	10
Error (kV primary)	3.7

C. *Two Simultaneous AG Faults With Synchronized and Unsynchronized Data*

Two simultaneous AG faults at 0.3 pu with $R_{AG1} = 20$ ohms primary and 0.7 pu with $R_{AG2} = 10$ ohms primary are simulated. A multivariate Newton-Raphson algorithm is used to solve with synchronized data (see results in Table VIII), and a genetic algorithm is used to solve with unsynchronized data (see results in Table IX). The genetic algorithm yields less accurate fault resistance calculations than the Newton-Raphson method does, but the calculated values still match the true values to within a factor of two. The calculated error value for the genetic algorithm solution is correspondingly higher as well.

TABLE VIII
SIMULTANEOUS AG FAULTS—NEWTON-RAPHSON SOLUTION RESULTS WITH SYNCHRONIZED DATA

Calculated Fault Parameters	Results of Newton-Raphson Solution
m_{AG1} (pu)	0.30
m_{AG2} (pu)	0.71
R_{AG1} (ohms primary)	19
R_{AG2} (ohms primary)	11
Error check (kV primary)	0.93

TABLE IX
SIMULTANEOUS AG FAULTS—GENETIC ALGORITHM SOLUTION RESULTS WITH UNSYNCHRONIZED DATA

Calculated Fault Parameters	Results of Genetic Algorithm Solution
m_{AG1} (pu)	0.34
m_{AG2} (pu)	0.71
R_{AG1} (ohms primary)	15
R_{AG2} (ohms primary)	15
Error check (kV primary)	5.3

VII. ANALYSIS OF AN EVOLVING FAULT ON AVISTA'S 115 KV TRANSMISSION SYSTEM

On January 13, 2021, a severe windstorm swept through the Inland Pacific Northwest. Avista saw over 130 total breaker operations throughout its system, with around 37 operations on the transmission network. One of the transmission faults occurred on a 115 kV line in the central portion of the Idaho panhandle. The line is 45 miles long and has three distribution substations tapped off it, as shown in Fig. 8. Motor-Operated Air Switch (MOAS) A is normally open and MOAS B is normally closed, creating two radial lines.

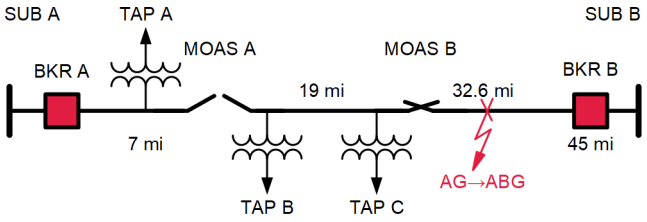

Fig. 8. Faulted 115 kV line configuration.

At 7:23 a.m., a 700 A AG fault developed at the 32.6 mile marker on the section of line fed by Substation B ($m = 0.28$ pu from Substation B, as confirmed by the line crew). The fault magnitude and fault resistance initially prevented the relay elements 67G1 and 21G1 (quad) from asserting. Five cycles after fault inception, B-phase faulted (950 A) while the A-phase fault persisted, and then the ground current surpassed the 67G1 pickup level (1,140 A) allowing the relays to trip the breaker. When Breaker B began to open, the A-phase fault current was 2.3 kA, and the B-phase fault current was 1.6 kA. The relay autoreclosed the breaker back into the ABG fault. However, this time the A-phase fault current was 1.4 kA, and the B-phase fault current was 1.9 kA. The relays immediately tripped the breaker to lock out on their switch onto fault logic.

Following the lockout, Avista personnel opened MOAS B and closed MOAS A to pick up the Tap B and C loads from Substation A. Later in the day, a line crew found the A- and B-phase conductors near Structure 32/3 (mile 32.6, or 0.28 pu from Substation B) lying on the ground with a tree on top of them. The center pole (holding B-phase) of Structure 32/3 was split at the top from the conductor getting pulled down. The crew was able to make the temporary repair shown in Fig. 9 using a distribution cross arm to reattach the insulator strings. The following month, a crew replaced the entire wooden structure with a steel design.

Fig. 9. Structure 32/3 temporary repair.

The first event report from Substation B (prior to the breaker opening) contains both the initial AG fault waveform data and the ABG fault data. The relay fault identification logic declared the fault to be of type AG because most of the event report data

were recorded during the period prior to B-phase becoming involved.

Before presenting the quantitative analysis of the first event report (prior to reclosing), we outline some tentative conclusions about the nature of the fault that are in harmony with the quantitative results:

1. The fault began as type AG when a tree fell on the line.
2. The tree made contact with the B-phase five cycles later, causing the fault to evolve into a nonstandard ABG topology. The A-phase was the outermost conductor on the line, with the B-phase in the middle, making this a plausible scenario.
3. With the A-phase and B-phase involved, the resistance from the A-phase to the ground was considerably smaller than the resistance from the B-phase to the A-phase. This may be because the relatively thick, bare tree trunk was in contact with the A-phase while a smaller branch with needles was in contact with the B-phase, providing additional resistance.

Fig. 10 illustrates the scenario described in Point 3, albeit in an oversimplified way. The fault on the left is equivalent to simultaneous AG and BG faults at the same location, which is a special case of T2 described in Section IV. It is also equivalent to a special case of ABG T1 described in Section III in which R_A and R_G are small compared to R_B. Thus, for this fault, T1 and T2 converge, and the following quantitative results demonstrate this convergence.

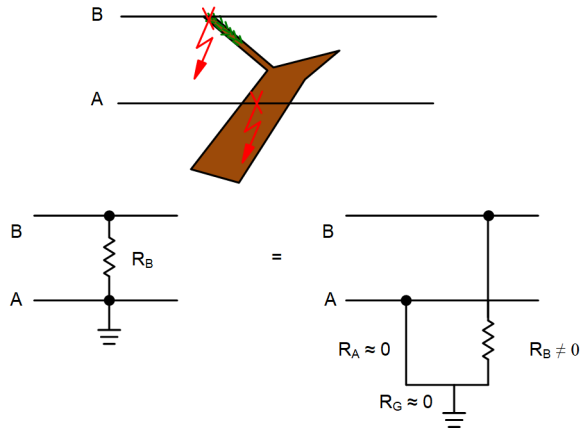

Fig. 10. Proposed scenario for a fallen tree causing a nonstandard ABG fault.

To test the DLG fault location algorithms proposed in this paper against the field data and against traditional DLG algorithms, we can process the event report data using a general-purpose programming language to derive results. Because the fault is on a radial line and only one event report is available, no data synchronization is required.

The following methods are used:

1. A traditional negative-sequence polarized AG fault locator analyzes the AG fault period within the first event report. The per-unit fault location output of this algorithm is referred to as m_{AG_IA2}.
2. A traditional negative-sequence polarized ABG fault locator ($I_{pol} = I_{AB2} = I_{A2} - I_{B2}$) analyzes the ABG faults before and after reclosing. The per-unit fault location output of this algorithm is referred to as m_{ABG_IAB2}.
3. A traditional loop-current polarized ABG fault locator ($I_{pol} = I_{AB} = I_A - I_B$) analyzes the ABG faults before and after reclosing. The per-unit fault location output of this algorithm is referred to as m_{ABG_IAB}.
4. The generalized DLG fault location algorithm from Section III (T1) adapted for a radial line by setting the remote current values to zero. The outputs of this algorithm are the per-unit fault location m_{ABG_T1} and fault resistances R_{A_T1}, R_{B_T1}, and R_{G_T1}. Quality checks cannot be performed in this case because the line is radial and only one event report is available. The calculated m_{ABG_T1} and R_{A_T1} values are meaningful after the inception of the AG fault. The calculated R_{B_T1} value is meaningful after B-phase becomes involved in the fault.
5. The generalized DLG fault location algorithm from Section IV (T2) adapted for a radial line by setting the remote current values to zero. The outputs of this algorithm are the per-unit fault locations m_{AG_T2} and m_{BG_T2} and fault resistances R_{AG_T2} and R_{BG_T2}. Quality checks cannot be performed in this case because the line is radial and only one event report is available. During the AG fault period, m_{AG_T2} and R_{AG_T2} are calculated using a 2 by 2 linear system. The m_{BG_T2} and R_{BG_T2} values are only meaningful after B-phase becomes involved in the fault.

Fig. 11 shows the primary currents and voltages during the first event. The AG fault occurs approximately 3.5 cycles into the event and the B-phase becomes involved approximately 8.5 cycles into the event.

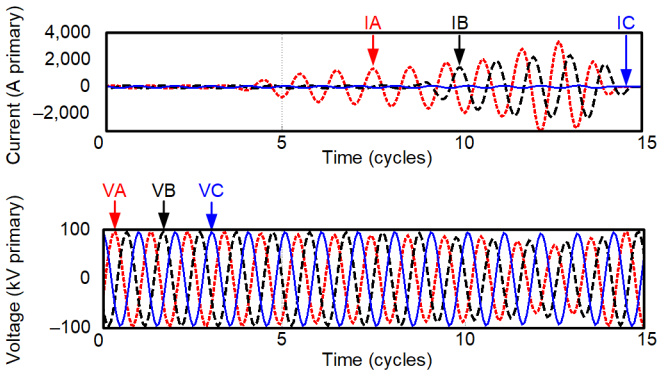

Fig. 11. Primary currents and voltages for the first event.

The per-unit fault location results from the various methods are shown in Fig. 12. The fault location algorithms are run on every data sample from the event report. The plot begins at the inception of the AG fault and ends just before the breaker opens.

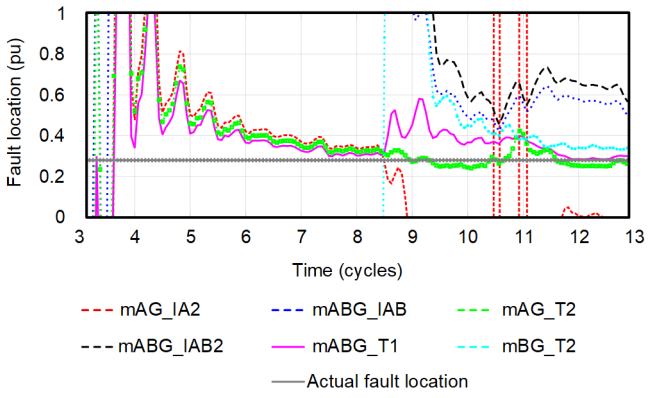

Fig. 12. Calculated per-unit fault locations (first event).

The primary fault resistance results associated with T1 and T2 are shown in Fig. 13. The plot begins at the inception of the AG fault and ends just before the breaker opens. Prior to the involvement of B-phase in the fault, the values of R_{B_T1} and R_{BG_T2} are much larger than the values of R_{A_T1} and R_{AG_T2}, as expected.

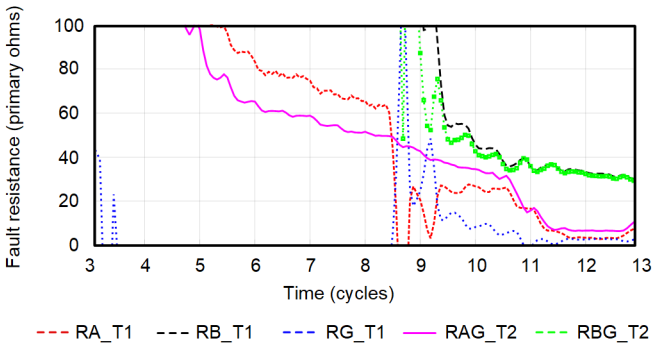

Fig. 13. Calculated primary fault resistances for T1 and T2 (first event).

The following are some key observations from the quantitative fault analysis results:

1. During the AG fault period (after some settling of transients), all three related fault location values (m_{ABG_T1}, m_{AG_T2}, and m_{AG_IA2}) are around 0.3 to 0.35 per unit, which agrees reasonably well with the 0.28 per unit fault location reported by the field crew.
2. When B-phase becomes involved, the negative-sequence polarized AG fault locator (m_{AG_IA2}) yields unreliable results because its polarizing quantity becomes corrupted. Quantities m_{ABG_T1} and m_{AG_T2} remain relatively unaffected.
3. After the fault evolves, the standard negative-sequence polarized and loop-current polarized ABG fault locators (m_{ABG_IAB2} and m_{ABG_IAB}, respectively) yield values between 0.55 and 0.7 per unit. These values differ considerably from the known AG fault location value (0.28 per unit), suggesting that the fault evolved into a nonstandard ABG topology, resulting in m_{ABG_IAB2} and m_{ABG_IAB} having incorrect values.
4. By contrast, the results of the fault location methods presented in this paper (m_{ABG_T1}, m_{AG_T2}, and m_{BG_T2}) all agree reasonably well with each other during the ABG fault period. They also agree with the previous AG fault location result and with the location reported by the field crew. These methods yield values between 0.25 and 0.35 per unit. T1 and T2 converge for this event, and the fault appears to consist of an AG fault and a BG fault at the same location. Recall that in T2, the AG and BG fault locations are not required to be the same, although they were in this case.
5. Calculated fault resistances R_{A_T1}, R_{G_T1}, and R_{AG_T2} are small compared to R_{B_T1} and R_{BG_T2}, serving as further evidence of the convergence between T1 and T2 for this fault.

After reclosing four seconds later, there was fault current on A-phase and B-phase as shown in Fig. 14, indicating the continued presence of the ABG fault. This correlates with the two conductors the crew found lying on the ground because the conductors had time to fall during the pole-open interval. In Fig. 14, the time axis reflects the fact that reclosing occurred approximately four seconds (≈ 240 cycles) after the beginning of the first event. The A-phase fault current was substantially lower than its previous value and closer in magnitude to the B-phase current following reclose, and the calculated A-phase fault resistance was correspondingly higher and closer in value to B-phase's fault resistance (Fig. 15), which one would expect with both conductors contacting the ground after initially being in contact with different portions of the tree. After the reclose, the outputs of traditional fault locators (m_{ABG_IAB2} and m_{ABG_IAB}) are much closer to the actual fault location than before (see Fig. 16), and the fault location results for T1 and T2 (m_{ABG_T1}, m_{AG_T2}, and m_{BG_T2}) are somewhat less accurate than before. The resistance plots once again illustrate the convergence between T1 and T2 ($R_{G\_T1} \approx 0$, $R_{A\_T1} \approx R_{AG\_T2}$, $R_{B\_T1} \approx R_{BG\_T2}$), indicating that the fault still appeared as AG and BG faults in the same location after reclosing.

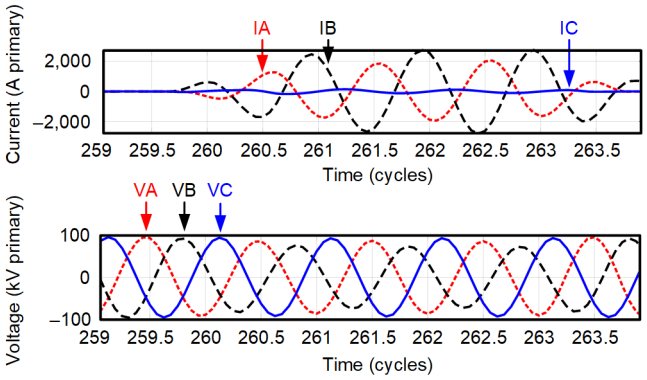

Fig. 14. Primary current and voltages after reclosing.

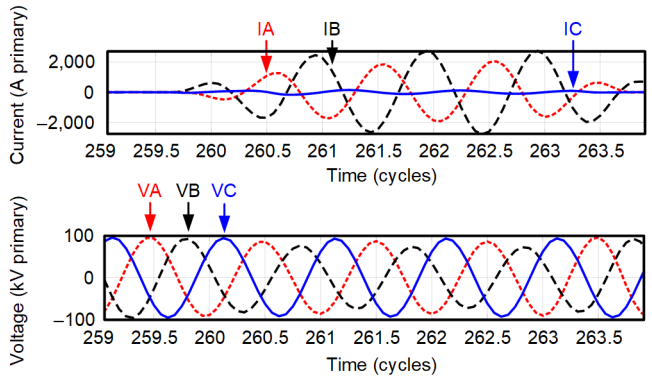

Fig. 15. Calculated primary fault resistances to T1 and T2 (after reclosing).

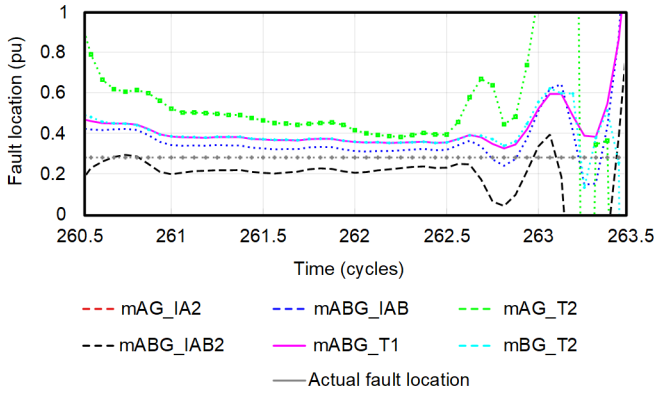

Fig. 16. Calculated per-unit fault locations after reclosing.

The resistance results from T1 and T2 may help to explain why the traditional ABG fault locator results are much more accurate after reclosing than before reclosing. As discussed in Section I, when the fault corresponds to T1 and $R_A \approx R_B$, the loop-current polarized ABG fault locator yields accurate results. The resistance plots in Fig. 15 indicate that this was roughly the case after reclosing, in contrast to the very different A-phase and B-phase resistances calculated from the first event report.

VIII. Conclusion

Complex DLG faults can be solved using phase domain methods that naturally incorporate fault resistance into the solution. These methods use event report data from both ends of the transmission line. Synchronized data (e.g., GPS time signals present at both line ends) allow for linear algebra solutions. Iterative solution methods are required when the data are unsynchronized or when the same phase is faulted at multiple locations within the protection zone. Radial lines do not require synchronized data or iteration, and they can be analyzed with modified versions of the general solutions (with the remote currents set to zero). The proposed algorithms include quality checks that can be used to confirm the fault topology. This paper demonstrates the applicability of the proposed methods to a real-life ABG fault with a nonstandard topology.

IX. References

[1] J. J. Grainger and W. D. Stevenson, *Power System Analysis*. McGraw Hill, New York, NY, 1994.

[2] J. D. Glover, M. S. Sarma, and T. J. Overbye, *Power System Analysis and Design*, Cengage Learning, Boston, MA, 2007.

[3] P. M. Anderson, "Changes in Symmetry," in *Analysis of Faulted Power Systems*, Wiley-IEEE Press, New York, NY, 1995, pp. 273–307. Available: doi 10.1109/9780470544129.ch8.

[4] D. Novosel, D. G. Hart, E. Udren, and J. Garitty, "Unsynchronized Two-Terminal Fault Location Estimation," in *IEEE Transactions on Power Delivery*, Vol. 11, Issue 1, January 1996, pp. 130–138. Available: doi 10.1109/61.484009.

[5] M. L. Crow, *Computational Methods for Electric Power Systems*, CRC Press, Boca Raton, FL, 2010.

[6] F. Solomonese, C. Barbulescu, S. Kilyeni, and M. Litcanu, "Genetic Algorithms. Power Systems Applications," proceedings of the *2013 6th International Conference on Human System Interactions (HSI)*, Sopot, Poland, June 2013, pp. 407–414. Available: doi 10.1109/HSI.2013.6577856.

[7] Å. Björck, *Numerical Methods for Least Squares Problems*, SIAM, Philadelphia, PA, 1996.

X. Biographies

Steven Chase received his bachelor of science degree in electrical engineering from Arizona State University in 2008 and his master of science in electrical engineering degree in 2009. He worked for two years as a substation design intern at Salt River Project, an Arizona water and power utility. He joined Schweitzer Engineering Laboratories, Inc. (SEL) in 2010, where he works as a senior power engineer in the research and development division. He is currently a registered PE in the state of Washington.

Sumit Sawai received a bachelor's degree in electrical engineering from the Sardar Patel College of Engineering in Mumbai, India, in 2011 and a master's degree in electrical engineering from Michigan Technological University in Houghton, MI, in 2015. He joined Schweitzer Engineering Laboratories, Inc. (SEL) in 2015 and holds the position of lead power engineer in the research and development division. He is currently a registered PE in the state of Washington.

Douglas Taylor received his BSEE and MSEE degrees from the University of Idaho in 2007 and 2009. He joined Schweitzer Engineering Laboratories, Inc. (SEL) in 2009 and worked as a protection engineer and a research engineer in the Research and Development division. In 2019, Doug joined the System Protection group at Avista Utilities and currently serves as a senior protection engineer. He is a registered professional engineer in the state of Washington and a member of the WPRC planning committee. Doug's main interests are power system protection and power system analysis. He holds 3 patents and has coauthored over 20 technical papers in the area of power system protection.